Inorganic Chemistry

ARTICLE

pubs.acs.org/IC

Ionothermal Synthesis and Magnetic Studies of Novel Two-Dimensional Metal−Formate Frameworks

Paul J. Calderone,[†] Paul M. Forster,[⊥] Lauren A. Borkowski,[‡] Simon J. Teat,[#] Mikhail Feygenson,[▽] Meigan C. Aronson,[§,▽] and John B. Parise[*,†,‡,∥]

[†]Department of Chemistry, [‡]Mineral Physics Institute, Earth and Space Science Building, [§]Department of Physics and Astronomy, and [∥]Department of Geosciences, Earth and Space Science Building, Stony Brook University, Stony Brook, New York 11794, United States

[⊥]Department of Chemistry, University of Nevada Las Vegas, 4505 Maryland Parkway, Box 454003, Las Vegas, Nevada 89154-4003, United States

[#]Advanced Light Source, Lawrence Berkeley National Lab, 1 Cyclotron Road, mail stop 2-400, Berkeley, California 94720, United States

[▽]Condensed Matter Physics and Materials Science Department, Brookhaven National Laboratory, Upton, New York, 11973-5000, USA

Supporting Information

ABSTRACT: Five novel two-dimensional frameworks containing formate-bridged metal-centered octahedra are synthesized ionothermally from two ionic liquids previously unused as solvents in hybrid synthesis, 2-hydroxyethylammonium (HEA) formate, and 1-hydroxy-3-proplyammonium (HPA formate. Templating effects of the cation from each ionic liquid drive the formation of different structures. $[NH_3C_2H_4OH]_2[M(CHO_2)_4]$ (**1**: M = Co, **2**: M = Ni) exhibit the same stoichiometry and connectivity as their manganese analogue (**3**: M = Mn), but the manganese form exhibits a different topology from **1** and **2**. $[NH_3C_3H_6OH][M(CHO_2)_3(H_2O)]$ (**4**: M = Co, **5**: M = Mn) were synthesized using the HPA formate ionic liquid with a metal−formate connectivity related to those of **1**−**3**. Canted antiferromagnetic ordering occurs at low temperatures (**1**: T_N = 7.0 K, **2**: T_N = 4.6 K, **3**: T_N = 8.0 K, **4**: T_N = 7.0 K, **5**: T_N = 9.2 K), similar to the magnetic properties previously reported for other metal−formate hybrid materials.

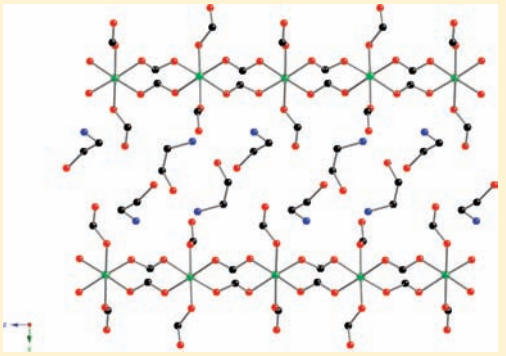

INTRODUCTION

Varied dimensionality and seemingly limitless linker possibilities[1,2] provide many opportunities for the design of functional inorganic−organic hybrid structures, such as metal−organic frameworks (MOFs). While much of the recent research into MOF materials has been driven by the design of low-density, high surface area frameworks for gas storage applications,[3−7] porosity is not the only property that shows significant promise for future applications. MOFs have also demonstrated, for example, useful optical[1,8] and catalytic[9,10] properties. In fact, many of the important behaviors associated with transition metal oxides, such as electronic conductivity and magnetic ordering,[11] are now known to occur in MOFs as well.[12,13]

Magnetic properties of transition metal MOFs offer great potential for exploration and are of paramount importance is choosing short ligand bridges to effectively and efficiently transfer magnetic coupling between metal atoms.[14] Following this principle, examples of formate-bridged 3d transition metal systems utilizing short $HCOO^-$ metal connections have emerged as a means to construct new molecular magnets.[15−20] Cheetham and co-workers' recent discovery of a series of multiferroic MOFs based on transition metal−formates has created an even greater interest in the prospective uses of new MOF materials.[21] Multiferroic materials exhibit both magnetic and ferroelectric ordering, and the occurrence of both properties in the same compound is especially interesting in MOFs because only a small number of purely inorganic materials had previously been recognized as multiferroic.[22,23]

Given the success that reticular chemistry has achieved at envisioning and subsequently synthesizing new MOFs topologies, multiferroicity presents yet another property that can be considered in the targeting of new structures. In metal−formate MOFs, for example, the final structure and properties are often determined by the templating effects of organocations that are incorporated into the framework. This is well-documented in the formate-based transition metal multiferroics described by Cheetham which adopt an ABX_3 perovskite-type topology. In these compounds, multiferroic behavior occurs due to a ferroelectric order−disorder transition involving the ammonium cation (located at the A-site in the structure) and magnetic ordering between octahedral metal atoms (B-sites).[21] This cation order−disorder transition was further investigated by Sánchez-Andújar et al., finding that hydrogen-bonding of the charge-balancing

Received: August 2, 2010
Published: February 11, 2011

Table 1. Crystallographic Data for 1−5

	1	2	3	4	5
chemical formula	$C_8H_{20}CoN_2O_{10}$	$C_8H_{20}NiN_2O_{10}$	$C_8H_{20}MnN_2O_{10}$	$C_6H_{15}CoNO_8$	$C_6H_{15}MnNO_8$
formula weight	363.19	362.97	359.20	288.12	284.13
crystal system	monoclinic	monoclinic	monoclinic	orthorhombic	orthorhombic
space group	$P2_1/n$ (No. 14)	$P2_1/n$ (No. 14)	$P2_1/c$ (No. 14)	*Pbca* (No. 61)	*Pbca* (No. 61)
a (Å)	6.866(1)	6.879(4)	8.925(9)	8.130(8)	8.270(7)
b (Å)	22.354(3)	22.363(1)	8.702(9)	16.131(1)	16.293(1)
c (Å)	9.582(1)	9.522(5)	9.230(1)	16.780(1)	17.015(1)
α (deg)	90	90	90	90	90
β (deg)	90.272(4)	90.362(1)	98.405(2)	90	90
γ (deg)	90	90	90	90	90
V (Å^3)	1470.7(4)	1464.7(1)	709.1(1)	2200.7(4)	2292.8(3)
Z	4	4	2	8	8
λ	0.71073	0.71073	0.77490	0.77490	0.77490
D_{calcd} (g cm^{-3})	1.640	1.646	1.682	1.739	1.646
μ (mm^{-1})	1.218	1.376	1.835	2.000	1.485
temp (K)	298	298	100	150	90
R1 (on F_o^2, $I > 2\sigma(I)$)	0.0491	0.0311	0.0204	0.0262	0.0263
wR2 (on F_o^2, $I > 2\sigma(I)$)	0.0785	0.0783	0.0557	0.0720	0.0715

ammonium cation was a direct contributor to a low-temperature structural phase transition and the ferroelectric ordering.[24] A similar ferroelectric behavior has also been observed in the $[NH_4][Zn(HCOO)_3]$ system by Xu and co-workers.[25] Clearly, to better elucidate the nature of metal−formate framework systems, the effects that are created when the properties of ammonium cations are varied within a series must be studied. While previous attempts have explored variations of alkylammonium cations,[17,18] a more complete study can be carried out by varying the cation through changing alkyl chain length or adding functional groups, leading to the synthesis of related structure types.

Ionothermal synthesis is a relatively new synthetic strategy in the production of MOFs but can be uniquely tailored for the synthesis of metal formates containing extra-framework cations. Morris et al. first utilized the cationic component of an ionic liquid as a template for zeolite synthesis.[26] It is now known that with the ionothermal method, both the cation and the anion may serve as solvent, ligand template, and structure directing agent.[27] Tuning the ionic liquid components by selecting the desired cationic or anionic species has resulted in many interesting products, both inorganic[28−30] and hybrid,[31,32] including a chiral coordination polymer[33] and two perfluorinated aliphatic dicarboxylate hybrids.[34] Here, we demonstrate that ionothermal synthesis also provides a simple, effective, and versatile approach to the discovery of new magnetic metal−formate frameworks.

We have chosen to explore the synthesis of hydroxyammonium metal formate MOFs utilizing two ionic liquids of hydroxyammonium cations and the formate anion, both of which can be easily produced in any laboratory. The two ionic liquids used in this work are derived from the inexpensive, readily available reagents formic acid and the amino alcohols, 2-aminoethanol and 3-amino-1-propanol. A previous report has characterized a 2-hydroxyethylammonium formate ionic liquid derived from formic acid and 2-aminoethanol.[35] Here, we use related ionic liquids to synthesize formate-bridged magnetic MOFs based on Co, Ni, and Mn, finding that these ionic liquids offer the potential to act as solvent, organocation template source, and ligand source. We also compare the new frameworks generated in our ionic liquids to existing perovskite metal formates, finding that in the case of hydroxyammonium cations, templating effects and additional hydrogen bonding interactions drive structural dimensionality changes and lead to ordered structures with no potential for ferroelectric transitions.

RESULTS AND DISCUSSION

Syntheses. Ionic liquids were prepared by reacting formic acid with either 2-aminoethanol or 3-amino-1-propanol in a 1 dram to form 2-hydroxyethylammonium (HEA) formate or 1-hydroxy-3-proplyammonium (HPA) formate, respectively. The resulting liquid was stirred and allowed to cool to room temperature before adding metal source. Metal sources were added to the cooled liquid and the reaction was allowed to proceed in a capped vial in an oven.

Structure Descriptions and Considerations. Where the multiferroic formates reported by the Cheetham group can be described based on the perovskite structure, compounds **1**−**5** resemble n = 1 Ruddlesden−Popper phases (Table 1).[11] Compounds **1**−**3**, $[NH_3C_2H_4OH]_2[M(CHO_2)_4]$ (M = Co, Ni, Mn, respectively), consist of two-dimensional metal−formate nets created by formates bridging from the equatorial positions of the metal octahedra (Figure 1). Two nonlinking formates coordinate in the axial positions of the metal octahedra, and the terminal oxygen atoms extend in between the layers. Two HEA cations sit in between the anionic layers to serve as charge balance (Figures 2 and 3). Compounds **1** and **2** are isostructural with each other, but **3**, which shares the same stoichiometry and connectivity, exhibits a distinct structure as can be seen by comparison of Figures 2 and 3. Compounds **4** and **5**, $[NH_3C_3H_6OH][M(CHO_2)_3(H_2O)]$ (M = Co and Mn, respectively), are two-dimensional networks exhibiting a similar overall connectivity to that seen in **1**−**3** (Figure 1). However, only one nonlinking formate group occupies an axial position of the octahedron rather than two as for **1**−**3**. The remaining axial position is occupied by a bound water molecule while one HPA cation, required for charge balance, occupies the space between the layers (Figure 4). For compounds **1**−**5**,

dx.doi.org/10.1021/ic1015548 |*Inorg. Chem.* 2011, 50, 2159–2167

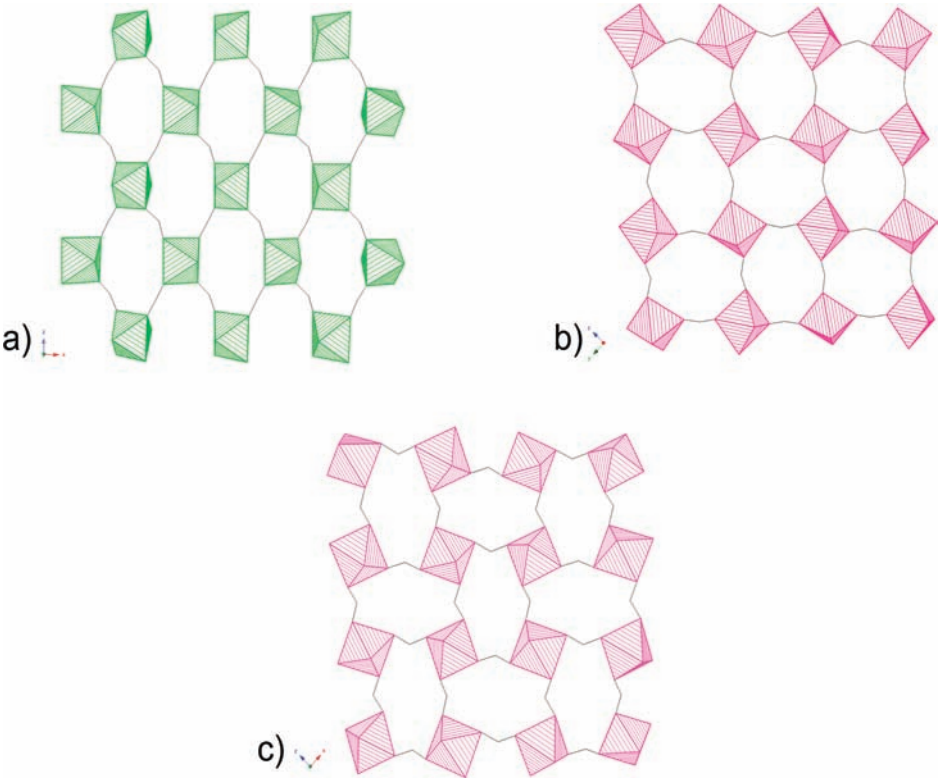

Figure 1. View of illustrating the different two-dimensional metal−formate−metal nets seen in **1** and **2** (a), **3** (b), and **4** and **5** (c). The networks are shown as metal octahedra bridged by wire bond formates. Network (a) is viewed in the [010] direction, (b) in the [100] direction, and (c) in the [010] direction.

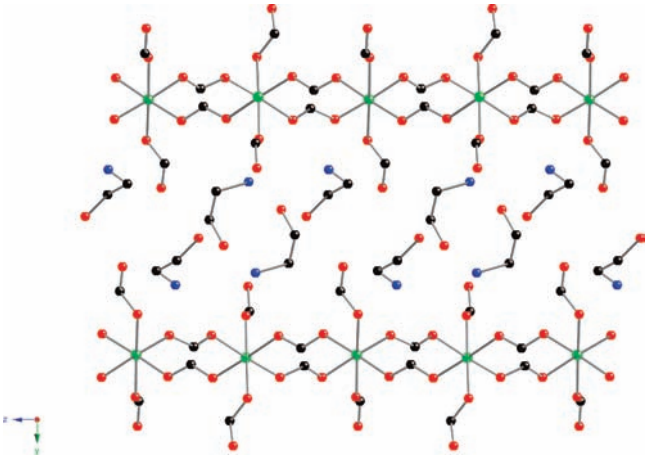

Figure 2. Illustration looking into the metal−formate network layers in **1** and **2** as viewed in the [100] direction. Nonlinking formate groups extend from the axial positions to interact with HEA cations between the layers. Metal atoms are shown in green. C atoms are in black. O atoms are shown in red. N atoms are shown in blue.

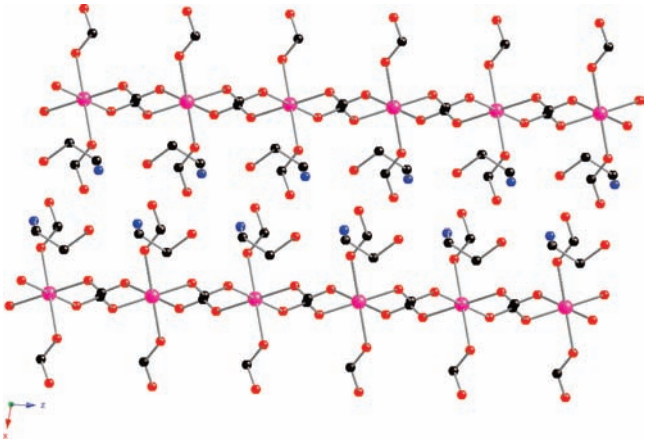

Figure 3. Illustration of **3** in the [010] direction looking into Mn−formate network layers. Nonlinking formates extend from axial positions of the octahedra to interact with HEA cations in the layers. Mn atoms are shown in pink. C atoms are shown in black. O atoms are in red. N atoms are in blue.

hydrogen-bonding interactions are observed between the nonlinking formate oxygen and the protonated ammonium group, as summarized in Supporting Information, Table S2. These hydrogen-bonding interactions are more numerous and presumably lead to greater stabilization than observed for 3D perovskite formates due both to the presence of additional groups on the cations capable of hydrogen bonding as well as the presence of uncoordinated formate oxygen atoms.

In this work, we present an alternative route to the synthesis of magnetic metal−formate MOFs through the use of formate-based ionic liquids, allowing us to better investigate the role of hydroxyammonium cations on the resulting formate structures. To our knowledge, these formate-bridged MOFs are the first examples where structures are produced from an ionic liquid providing both the bridging ligand as well as the extra-framework cation. All of the structures obtained in our experiments are two-dimensional, layered

dx.doi.org/10.1021/ic1015548 |*Inorg. Chem.* 2011, 50, 2159–2167

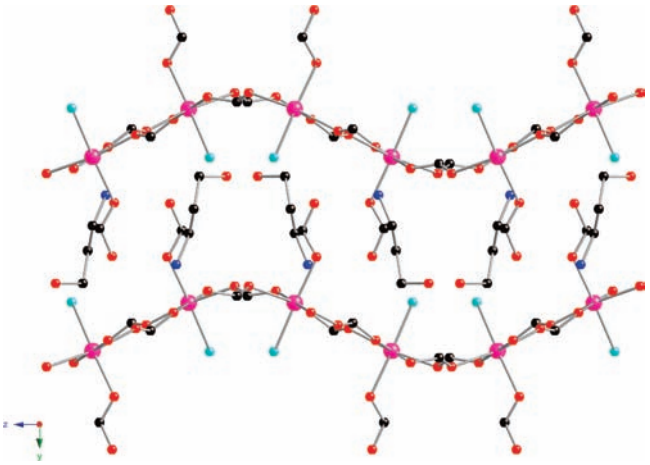

Figure 4. View of [100] direction looking into the distorted metal−formate layers of **4** and **5**. Nonlinking formate groups coordinated to an axial position interact with HPA cations in the layers while a bound water molecule occupies the other axial position. Metal atoms are shown in violet. C atoms are shown in black. O atoms are in red. N atoms are in blue. Water molecules are represented in aqua.

compounds, which is contrary to the three-dimensional frameworks produced when the templating effect of alkylammonium cations was investigated. When alkylammonium cations were used, the now well-established three-dimensional metal−formate connectivity resulted based on both the size and the limited hydrogen bonding character of the extra-framework cations.[15−18] However, this study utilizing hydroxyammonium cations and ionothermal synthesis found two-dimensional metal−formate layers formed with extensive hydrogen bonding between the nonbridging formates and the hydroxyammonium ions. This is unlikely to be due to a factor of size or chain length, as both alkylammonium and hydroxyammonium cations are of comparable size. Instead, increased framework-cation hydrogen-bonding interactions stabilize the 2D structure.

In comparison to the 3D formates cited above,[20] the 2D formates also follow a 2.11 *anti*−*anti* linking mode (Figure 1). The principle difference between the two structure types arises from the nonbridging formates, preventing 3D connectivity (Figures 2−4). As a result, the hydroxyammonium cations of each compound do not sit inside pores, as in the three-dimensional structure, but instead occupy space between two-dimensional formate nets. The size of the ionic liquid cation also influences the topology. A logical assumption for the HPA cation, with an additional CH_2 group compared to HEA, would lead to an increase the interlayer spacing. However, the increased size appears to destabilize the structure type observed in **1**−**3** in favor of one where half of the terminal formate anions are replaced by neutral water molecules. Consequently, only half as many HPA cations are needed to balance charge, leading to a smaller interlayer spacing and a distortion of the 2D nets to accommodate the cation (Figure 4). It is also notable that when similar reactions were attempted with formate liquids derived from still larger amino alcohols, 4-amino-1-butanol and 5-amino-1-pentanol, the products obtained the well-known metal formate dihydrate structure type,[36−38] implying that these cations were too large to allow organocation-containing structures to form at all.

In contrast with a three-dimensional connectivity, where the tilts and bond lengths of the octahedra are inherently constrained, two-dimensional connectivity allows for more structural freedom. A comparison of the isostructures produced with the HEA formate, **1**−**3**, demonstrates larger structural variability between different metal atoms compared to the 3D structures. Differences can be seen clearly when the O−C−O connections between neighboring metal octahedra are approximated as linear bonds and torsion angles defined by the O−M−M−O connections measured. The average torsion angle between octahedra in **1** and **2** is 54.7° and 54.9°, respectively, while **3** has an average torsion angle of 29.3° between Mn octahedra. The positioning of the nonlinking formates is then directly affected in each structure, as an increase in octahedral torsion angles leads to an increase in distance between O atoms of the nonlinking formates. Furthermore, the orientation of ammonium cations that hydrogen-bond to the nonlinking formates affects interlayer stacking. The respective interlayer distances of **1** and **2** (12.42 Å and 12.44 Å) are significantly larger than the interlayer distance observed in **3** (8.925 Å).

Adjustments in the framework can also be made through distortions of the metal octahedra. As shown in Supporting Information, Table S1, the metal−oxygen bonds for **1** and **2** show a greater distortion along their respective axial planes—the location of the nonlinking formates—than those of **3**. The extent of distortion also has an effect on how the respective structures fit together. A different pattern of octahedral tilting is observed in **3**, causing the void spaces in the two-dimensional net to alternate orientation (Figure 1). This is not seen in **1** and **2**, as the void spaces are ordered uniformly throughout that network. This effect also gives rise to an increased metal to metal distance in **3** of 6.343 Å, nearly 0.5 Å more than **1** and **2**.

All five compounds crystallize in centrosymmetric space groups. Given that the extra-framework cations are ordered in each compound, there is no opportunity for a ferroelectric phase transition to occur. Ferroelectric transitions of the type observed for the 3D perovskite phases require either an ordered structure that occurs in a noncentrosymmetric space group or a structure containing disordered cations that might undergo an ordering transition at different temperatures. Thus, while **1**−**5** are not multiferroic, their magnetic properties may help us to better understand magnetic ordering in this class of materials.

Magnetic Properties. The temperature T and magnetic field H dependencies of the dc magnetizations $M(T,H)$ and the temperature dependencies of the real χ' and imaginary χ'' parts of the ac susceptibility $\chi(T)$ were measured for each of the five samples. The temperature dependencies of the FC and ZFC dc magnetizations are depicted in Figure 5. $M(T)$ generally appears to increase monotonically with decreasing temperature; however, the insets of Figure 5 suggest that magnetic order occurs in each of the samples at low temperatures. Separation of the FC and ZFC magnetizations is one indication of magnetic order, and this effect is particularly pronounced in samples **1** and **5** where the magnetic ordering temperatures are 7.0 and 9.2 K, respectively. The separation is less dramatic in samples **2**, **3**, and **4** where the separation of the FC/ZFC magnetizations occurs at 4.6 K, 8.0 K, and 7.0 K, respectively. These measurements of T_N are summarized in Table 2. The separation of the FC and ZFC magnetizations only reveals the presence of a net uncompensated moment in the ordered phase, such as those found in domain walls in the ordered state, and it does not unambiguously differentiate ferromagnetic ordering from a complex form of antiferromagnetic order, such as the canted antiferromagnetism that was previously reported in this class of compounds.[15,16,18,39] Antiferromagnetic phase transitions are distinguished by a peak in the temperature derivative of the real part of the ac susceptibility χ' at the Néel temperature T_N,[40] where an accompanying peak in the absorption, that is, the imaginary part of the susceptibility χ'', occurs,

dx.doi.org/10.1021/ic1015548 |*Inorg. Chem.* 2011, 50, 2159–2167

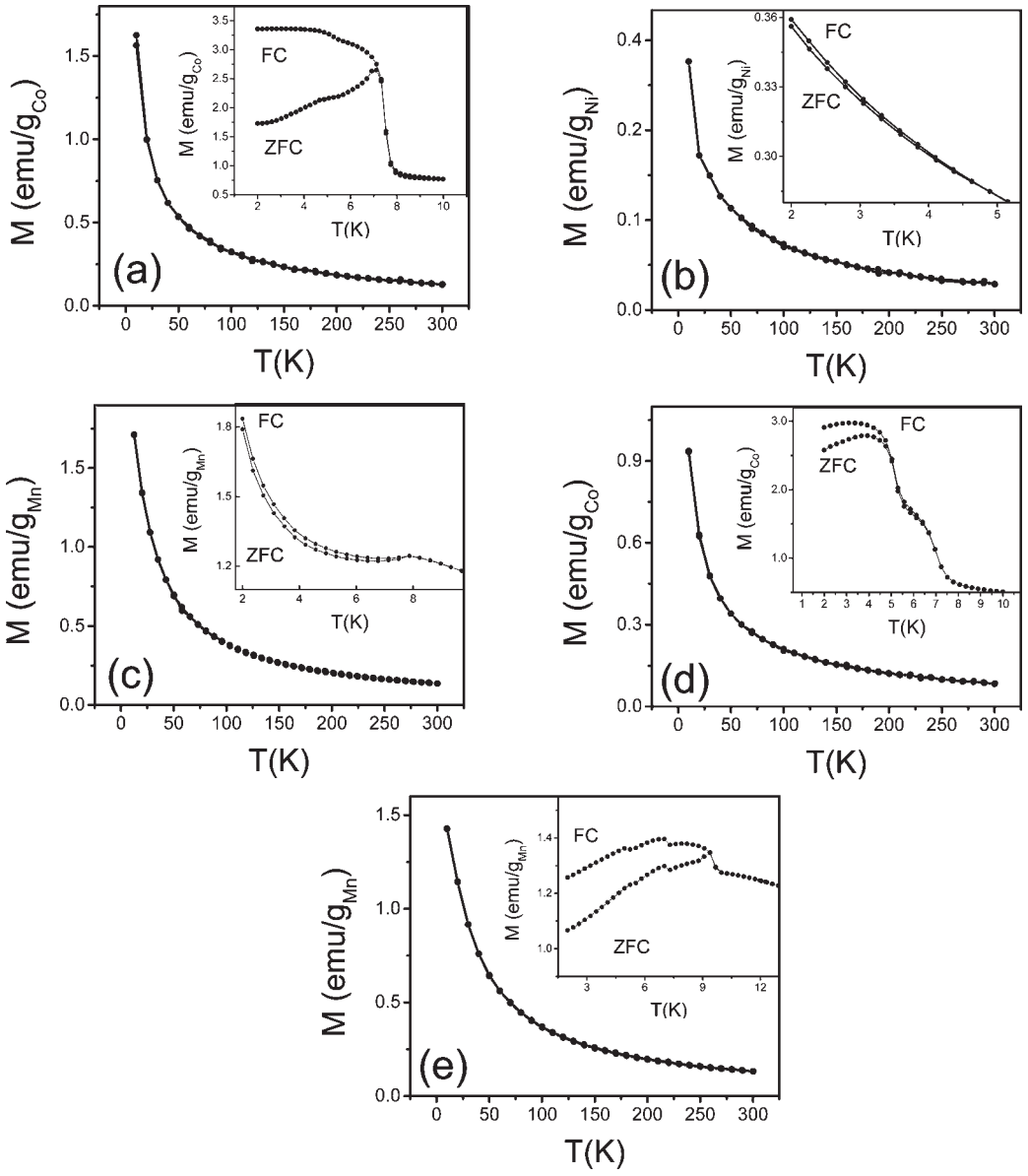

Figure 5. Temperature dependencies of the ZFC and FC magnetizations in a magnetic field of 500 Oe for samples (a) **1**, (b) **2**, (c) **3**, (d) **4**, and (e) **5**. Insets: expanded view of low temperatures regimes. The ZFC/FC separation in sample **4** is small but nonzero between 7 K and 5 K, where it becomes much larger (Inset, (d)).

Table 2. Summary of Magnetic Properties of Samples 1−5[a]

sample	T_N (K)	T_N* (K)	θ (K)	μ_{eff} (μ_B/atom)	μ_{th} (μ_B/atom)	M_S (μ_B)	M_S^{free} (μ_B)	H_C (Oe)
1 Co^{2+}	7.0	7.3 ± 0.1, 5.1 ± 0.1	−46	4.1	4.8	1.5	3	400
2 Ni^{2+}	4.6	1.9 ± 0.1	−33	3.3	3.2	0.3	2	700
3 Mn^{2+}	8.0	8.0 ± 0.15	−10	6.1	5.9	1.9	5	20
4 Co^{2+}	7.0	6.7 ± 0.15, 4.7 ± 0.1	−30	5.1	4.8	0.9	3	300
5 Mn^{2+}	9.2	9.6 ± 0.1	−14	6.1	5.9	1.6	5	100

[a] T_N is the magnetic ordering temperature defined from the separation of the FC and ZFC measurements of the dc magnetization, T_N* is the ordering temperature defined from ac susceptibility measurements, θ is the Weiss constant, μ_{eff} is the effective paramagnetic moment per metal atom, μ_{th} is the calculated theoretical value of μ_{eff}, M_S is the saturation magnetization at 2 K at 50 kOe, M_S^{free} is the calculated saturation magnetization, and H_C is the coercive field at 2 K.

reflecting the onset of either intrinsic or extrinsic slow modes at the onset of magnetic order, as well as the enhanced dissipation associated with relaxing these modes. Here, we will determine T_N from the maximum in $\chi''(T)$. The measurements of the temperature dependencies of χ' and χ'' for **1**−**5** are shown in Figure 6. In Co-based **1**, we observe a strong peak in χ' and a

dx.doi.org/10.1021/ic1015548 |*Inorg. Chem.* 2011, 50, 2159–2167

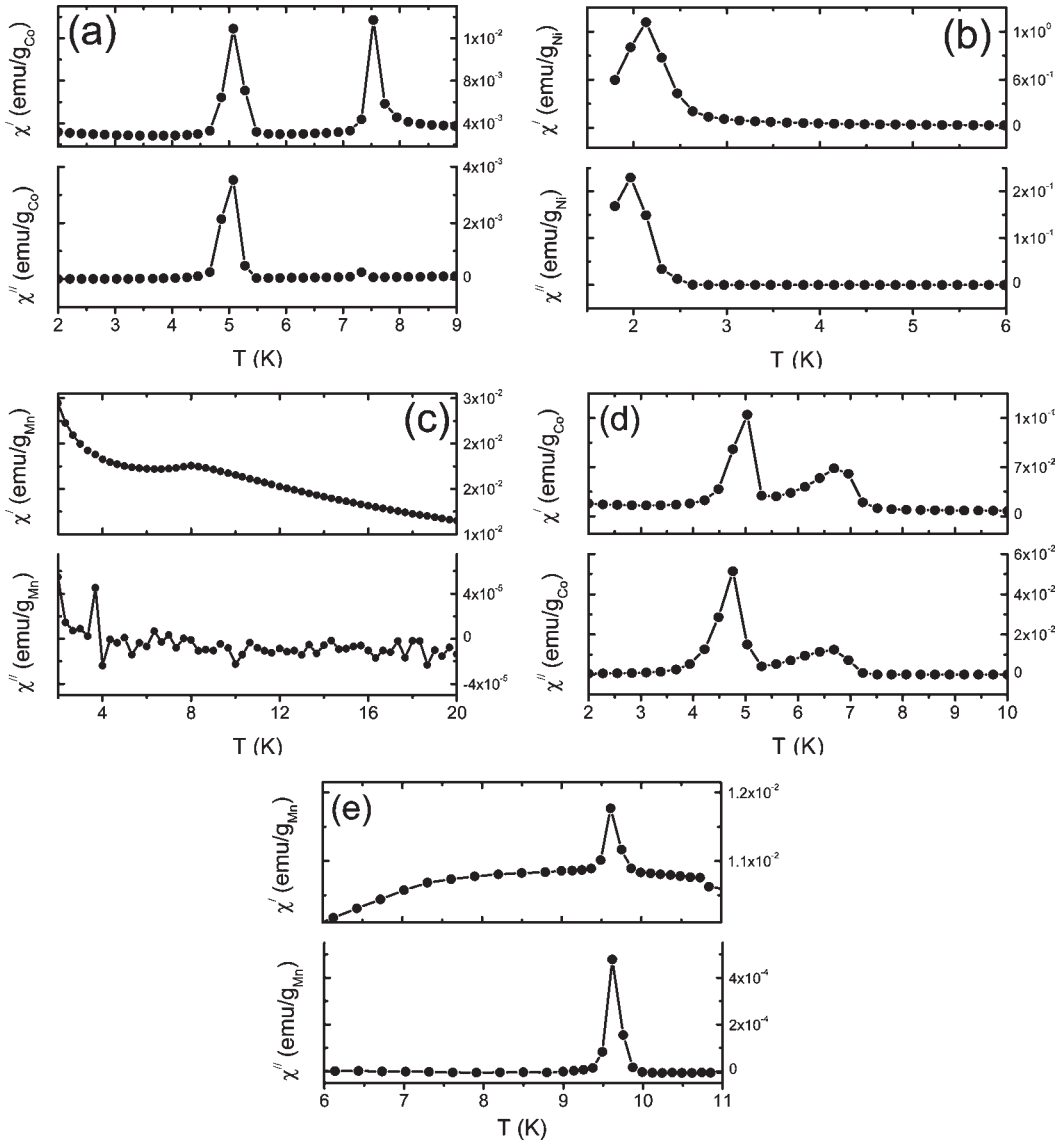

Figure 6. Temperature dependencies of the real part χ' and imaginary part χ'' of the ac susceptibility for samples (a) **1**, (b) **2**, (c) **3**, (d) **4**, and (e) **5**.

very weak peak in χ'' at 7.3 ± 0.1 K (Figure 6a), close to the temperature where the FC and ZFC magnetizations separate, but there are additional peaks in χ' and χ'' at 5.1 ± 0.1 K, where weak features are also found in the FC and ZFC magnetizations (Figure 5a, inset). Qualitatively similar observations are made in **4** (Figure 6d), which is also Co-based. While these additional transitions can be due to slight impurities in the samples, it is also possible the initial magnetic structure that appears at 7 K in **1** and **4** is unstable and transforms into a second structure at 5.1 K. This explanation was also used when a similar second transition was previously reported by Wang et al.[15] who proposed that this behavior corresponds to a net rotation of the uncompensated moment. As was also stated by Wang, definitive proof of this scenario awaits a determination of the magnetic structure by neutron diffraction measurements. Samples **2** and **5** show single magnetic transitions, where the peaks in $\chi''(T_N)$ occur very near the same temperatures where the FC and ZFC magnetizations separate in **5**, while we take the peak in $\chi''(T_N)$ to be a more accurate determination of the onset of order than the separation of the FC/ZFC magnetizations in **2**. No peak in χ'' is found in **3**, but the presence of a broad peak in χ' and a separation of the ZFC/FC magnetizations suggest that here, too, canted antiferromagnetism occurs at 8.0 ± 0.15 K. The peak in χ' is much broader in **3** than in the other compounds, and it is possible that the implied disorder may also reduce the population of slow modes in this sample.

The good agreement between the magnetic ordering temperatures determined from the ac susceptibility and FC/ZFC $M(T)$ measurements is summarized for all five samples in Table 2.

The temperature dependence of the dc susceptibility $\chi(T) = M(T)/H$, measured in a dc field H of 500 Oe, increases monotonically with decreasing temperatures, and for temperatures between 10 and 300 K is well described by the Curie−Weiss law, $\chi = C/(T - \theta)$. The values of $\chi = M/H$ are different from those determined by the ac susceptibility measurement, since the latter were performed in a 4 Oe oscillating field. We have plotted $1/\chi$ as a function of temperature in Figure 7, allowing us to determine the Curie constant C and the Weiss constant θ as parameters of straight line fits to these data. We calculated the effective paramagnetic moment $\mu_{eff} = (8C)^{1/2}$ of each metal ion using the

dx.doi.org/10.1021/ic1015548 |*Inorg. Chem.* 2011, 50, 2159–2167

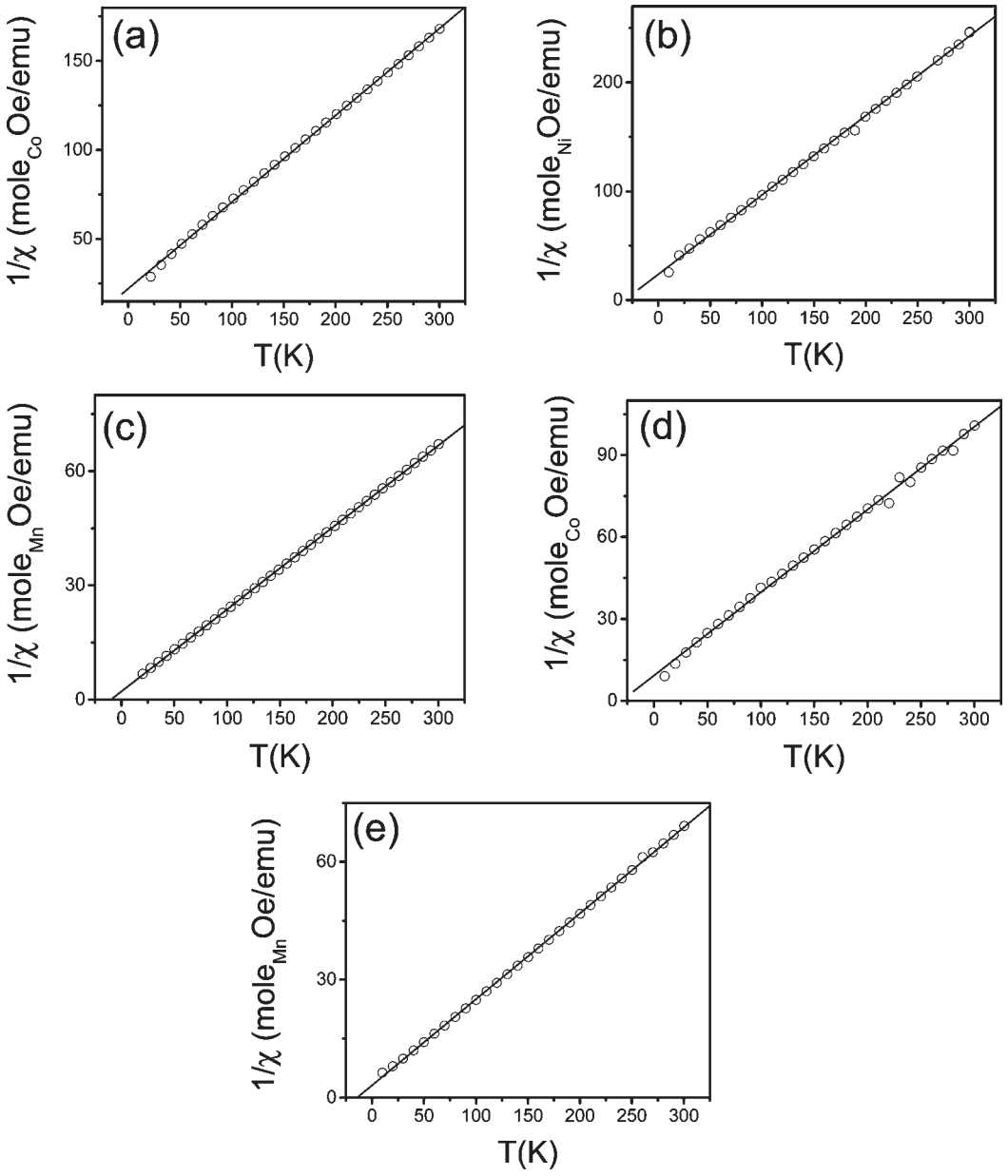

Figure 7. Inverse molar susceptibility χ as a function of temperature for samples (a) **1**, (b) **2**, (c) **3**, (d) **4**, and (e) **5**. The solid lines are the fits to Curie–Weiss expression, as described in the text.

measured values of C for each sample, and the results are compared to the previously reported values of μ_{eff} for Co^{2+}, Ni^{2+}, and Mn^{2+} in Table 2, showing good agreement. We find that the Weiss constant θ is negative for **1**–**5**, indicating that the mean field for the fluctuating moments is overall antiferromagnetic, supporting the conclusions of the ac susceptibility analyses, above.

The field dependence of the dc magnetization is different above and below the antiferromagnetic phase transition. Below T_N, the magnetization is almost linear at high magnetic fields (Figure 8), while at lower fields it is hysteretic with small coercive fields H_C (insets, Figure 8). No hysteresis was detected above T_N. The values of H_C for all samples are summarized in Table 2. At the lowest temperature (2 K) and highest applied field (50 kOe), the saturation magnetization M_S per metal ion is much smaller than the value calculated for the corresponding isolated metal ion $M_S = gJ\mu_B$, where g is a Landé factor and J is a total angular momentum (Table 2).

In summary, we have determined from measurements of the ac and dc susceptibility that all five metal formate samples are moment bearing and order antiferromagnetically below 10 K. The antiferromagnetic order is not simple, since the ordered state displays hysteresis between field cooled and zero field cooled magnetizations, as well as a pronounced coercive field. Our observations are consistent with earlier measurements that concluded that the ordered state of metal–formate hybrids can best be described as a canted antiferromagnet.

CONCLUSION

The five magnetic metal–formate frameworks presented here were synthesized ionothermally by utilizing two different ionic liquid solvents, hydroxyethylammonium (HEA) formate and 1-hydroxy-3-proplyammonium (HPA) formate. The use of HEA

dx.doi.org/10.1021/ic1015548 |*Inorg. Chem.* 2011, 50, 2159–2167

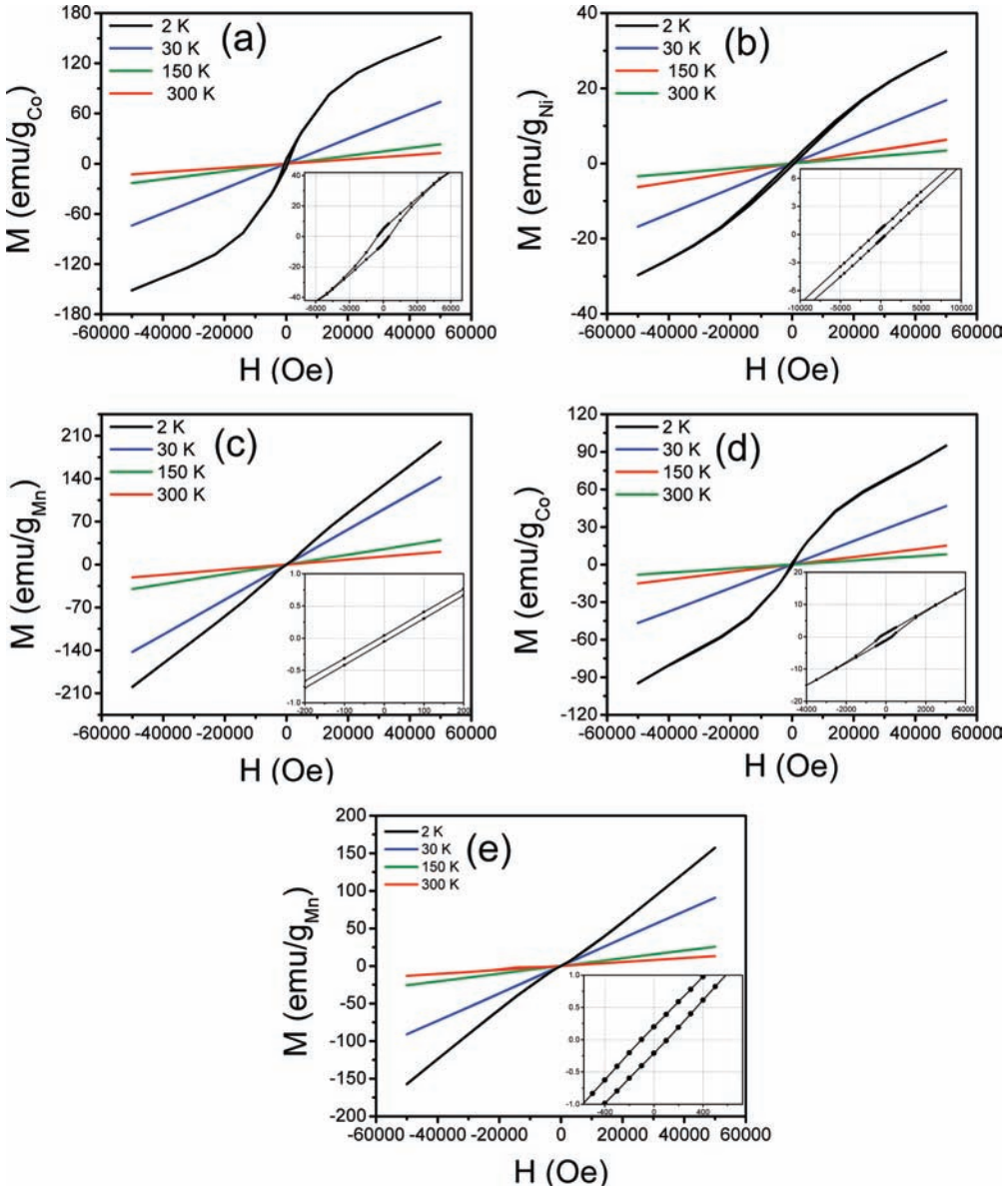

Figure 8. Magnetization *M* as a function of magnetic fields *H* at different temperatures for samples (a) **1**, (b) **2**, (c) **3**, (d) **4**, and (e) **5**. Insets: Expanded view of the low field magnetization at 2 K for samples (a) **1**, (b) **2**, (c) **3**, (d) **4**, and (e) **5**.

formate in **1**−**3** yielded a metal−formate network with two nonlinking formate groups in the axial positions, while using HPA formate in **4** and **5** produced a 2D metal−formate framework with the axial coordination sites occupied by one formate anion and a water molecule. In each compound, the ionic liquid cation is incorporated into the resulting structure as a charge balancing species, demonstrating that the choice of ionic liquid cation can greatly affect the resulting metal−organic framework. It was found that all samples can be classified as canted antiferromagnets, a magnetic behavior consistent with other previously reported magnetic metal formate hybrids. Minor reaction modifications, such as a change in metal center or ammonium cation, produced each compound described in this work, demonstrating that ionothermal synthesis of formate-based ionic liquids is a simple yet effective means for the discovery of new varieties of magnetic metal−formate frameworks. Future work will continue to utilize ionothermal methods in this system, targeting new multiferroic materials.

■ ASSOCIATED CONTENT

Supporting Information. Full experimental procedures and CIF files for compounds **1**−**5** as well as supplementary figures and tables. This material is available free of charge via the Internet at http://pubs.acs.org. Compounds **1**−**5** have been deposited at the Cambridge Crystallographic Data Centre with numbers CCDC 749488−749492.

■ AUTHOR INFORMATION

Corresponding Author
*E-mail: john.parise@sunysb.edu.

■ ACKNOWLEDGMENT

The authors would like to thank Debasis Banerjee for advice in structure solutions and Dr. Timothy Glotch of the SBU

Geosciences Department for use of the ATR to obtain IR spectra. This work is being funded by the Division of Materials Research of the National Science Foundation, Grant Number DMR-0800415. Work at Brookhaven National Laboratory (M.C.A. and M.F.) is carried out under the auspices of the U.S. Department of Energy, Office of Basic Energy Sciences, under Contract No. DE-AC02-98CH1886. The Advanced Light Source is supported by the Director, Office of Science, Office of Basic Energy Sciences, of the U.S. Department of Energy under Contract No. DE-AC02-05CH11231.

REFERENCES

(1) Rao, C. N. R.; Cheetham, A. K.; Thirumurugan, A. *J. Phys.: Condens. Matter* 2008, *20*, 083202.
(2) Cheetham, A. K.; Rao, C. N. R.; Feller, R. K. *Chem. Commun.* **2006**, 4780.
(3) Xiao, B.; Wheatley, P. S.; Zhao, X. B.; Fletcher, A. J.; Fox, S.; Rossi, A. G.; Megson, I. L.; Bordiga, S.; Regli, L.; Thomas, K. M.; Morris, R. E. *J. Am. Chem. Soc.* **2007**, *129*, 1203.
(4) Ferey, G. *Chem. Soc. Rev.* **2008**, *37*, 191.
(5) Forster, P. M.; Eckert, J.; Heiken, B. D.; Parise, J. B.; Yoon, J. W.; Jhung, S. H.; Chang, J. S.; Cheetham, A. K. *J. Am. Chem. Soc.* **2006**, *128*, 16846.
(6) Murray, L. J.; Dinca, M.; Long, J. R. *Chem. Soc. Rev.* **2009**, *38*, 1294.
(7) Collins, D. J.; Zhou, H. C. *J. Mater. Chem.* **2007**, *17*, 3154.
(8) Evans, O. R.; Lin, W. B. *Acc. Chem. Res.* **2002**, *35*, 511.
(9) Farrusseng, D.; Aguado, S.; Pinel, C. *Angew. Chem., Int. Ed.* **2009**, *48*, 7502.
(10) Forster, P. M.; Cheetham, A. K. *Top. Catal.* **2003**, *24*, 79.
(11) Rao, C. N. R.; Raveau, B. *Transition Metal Oxides*, 2nd ed.; Wiley-VCH, 1998.
(12) Kurmoo, M. *Chem. Soc. Rev.* **2009**, *38*, 1353.
(13) Zhang, W.; Ye, H. Y.; Xiong, R. G. *Coord. Chem. Rev.* **2009**, *253*, 2980.
(14) Wang, X. Y.; Wang, Z. M.; Gao, S. *Chem. Commun.* **2008**, 281.
(15) Wang, X. Y.; Gan, L.; Zhang, S. W.; Gao, S. *Inorg. Chem.* **2004**, *43*, 4615.
(16) Wang, Z. M.; Zhang, B.; Inoue, K.; Fujiwara, H.; Otsuka, T.; Kobayashi, H.; Kurmoo, M. *Inorg. Chem.* **2007**, *46*, 437.
(17) Wang, Z. M.; Zhang, B.; Otsuka, T.; Inoue, K.; Kobayashi, H.; Kurmoo, M. *Dalton Trans.* **2004**, 2209.
(18) Wang, Z. M.; Zhang, X. Y.; Batten, S. R.; Kurmoo, M.; Gao, S. *Inorg. Chem.* **2007**, *46*, 8439.
(19) Wang, Z. M.; Zhang, B.; Zhang, Y. J.; Kurmoo, M.; Liu, T.; Gao, S.; Kobayashi, H. *Polyhedron* **2007**, *26*, 2207.
(20) Wang, Z. M.; Hu, K. L.; Gao, S.; Kobayashi, H. *Adv. Mater.* **2010**, *22*, 1526.
(21) Jain, P.; Ramachandran, V.; Clark, R. J.; Zhou, H. D.; Toby, B. H.; Dalal, N. S.; Kroto, H. W.; Cheetham, A. K. *J. Am. Chem. Soc.* **2009**, *131*, 13625.
(22) Spaldin, N. A.; Fiebig, M. *Science* **2005**, *309*, 391.
(23) Hill, N. A. *J. Phys. Chem. B* **2000**, *104*, 6694.
(24) Sanchez-Andujar, M.; Presedo, S.; Yanez-Vilar, S.; Castro-Garcia, S.; Shamir, J.; Senaris-Rodriguez, M. A. *Inorg. Chem.* **2010**, *49*, 1510.
(25) Xu, G.-C.; Ma, X.-M.; Zhang, L.; Wang, Z.-M.; Gao, S. *J. Am. Chem. Soc.* **2010**, *132*, 9588.
(26) Cooper, E. R.; Andrews, C. D.; Wheatley, P. S.; Webb, P. B.; Wormald, P.; Morris, R. E. *Nature* **2004**, *430*, 1012.
(27) Parnham, E. R.; Morris, R. E. *Acc. Chem. Res.* **2007**, *40*, 1005.
(28) Parnham, E. R.; Morris, R. E. *J. Am. Chem. Soc.* **2006**, *128*, 2204.
(29) Parnham, E. R.; Morris, R. E. *J. Mater. Chem.* **2006**, *16*, 3682.
(30) Parnham, E. R.; Wheatley, P. S.; Morris, R. E. *Chem. Commun.* **2006**, 380.
(31) Liao, J. H.; Huang, W. C. *Inorg. Chem. Commun.* **2006**, *9*, 1227.
(32) Lin, Z. J.; Wragg, D. S.; Warren, J. E.; Morris, R. E. *J. Am. Chem. Soc.* **2007**, *129*, 10334.
(33) Lin, Z. J.; Slawin, A. M. Z.; Morris, R. E. *J. Am. Chem. Soc.* **2007**, *129*, 4880.
(34) Hulvey, Z.; Wragg, D. S.; Lin, Z. J.; Morris, R. E.; Cheetham, A. K. *Dalton Trans.* **2009**, 1131.
(35) Bicak, N. *J. Mol. Liq.* **2005**, *116*, 15.
(36) Osaki, K.; Nakai, Y.; Watanabe, T. *J. Phys. Soc. Jpn.* **1964**, *19*, 717.
(37) Krogman, K.; Mattes, R. *Z. Kristallogr.* **1963**, *118*, 291.
(38) Antsyshkina, A. S.; Guseinova, M. K.; Porai-Koshits, M. A. *J. Struct. Chem.* **1966**, *8*, 321.
(39) Wang, Z. M.; Zhang, B.; Kurmoo, M.; Green, M. A.; Fujiwara, H.; Otsuka, T.; Kobayashi, H. *Inorg. Chem.* **2005**, *44*, 1230.
(40) Fisher, M. E. *Philos. Mag.* **1962**, *7*, 1731.